ISBN: 978-3-95450-233-2 ISSN: 2673-5504 doi:10.18429/JACoW-SRF2021-SUPTEV009

DEVELOPMENT OF A NEW B-MAPPING SYSTEM FOR SRF CAVITY VERTICAL TESTS*

J. C. Wolff[1,2†], A. Goessel[1], W. C. A. Hillert[2], C. Mueller[1], D. Reschke[1], L. Steder[1], D. Tischhauser[1]
[1]Deutsches Elektronen-Synchrotron (DESY), Notkestraße 85, D-22607 Hamburg, Germany
[2]University of Hamburg, Luruper Chaussee 149, D-22761 Hamburg, Germany

Abstract

Magnetic flux trapped in the Niobium bulk material of superconducting radio frequency (SRF) cavities degrades their quality factor and the accelerating gradient. The sensitivity of the cavity to trapped magnetic flux is mainly determined by the treatment, the geometry and the Niobium grain size and orientation. To potentially improve the flux expulsion characteristics of SRF cavities and hence the efficiency of future accelerator facilities, further studies of the trapping behavior are essential. For this purpose a so-called B-mapping system to monitor the magnetic flux along the outer cavity surface of 1.3 GHz TESLA-Type single-cell SRF cavities is currently under development at DESY. Contrary to former approaches, this system digitizes the sensor signals already inside of the cryostat to extensively reduce the number of required cable feedthroughs. Furthermore, the signal-to-noise ratio (SNR) and consequently the measuring sensitivity can be enhanced by shorter analog signal lines, less thermal noise and the Mu-metal shielding of the cryostat. In this contribution the design, the development process as well as first performance test results of the B-mapping system are presented.

B-MAPPING SYSTEM DESIGN

Based on the first magnetometric-mapping approach at Helmholtz-Zentrum Berlin (HZB) [1] a B-mapping system using Anisotropic MagnetoResistive (AMR) sensors of type Sensitec AFF755B [2] is currently under development at DESY. These single-axis AMR-sensors are arranged in groups of three to enable spatial magnetic flux measurements. To hold the sensor-groups in a desired position, nine groups each are mounted on a so-called sensor-board shown in Fig. 1. In the final setup 48 sensor-boards will surround the cell of a 1.3 GHz TESLA-Type single-cell SRF cavity. Thus, in total, the magnetic flux distribution of the outer cavity surface can be mapped by 432 sensor-groups or 1296 sensors. This system will be included in the vertical test stand environment at DESY to continue former studies [3–7] investigating the impact of the cavity geometry, the field orientation, the pre-treatment and the material grain size on the quality factor and the gradient of SRF cavities. To measure the magnetic flux directly on the cavity surface, a preferably low distance between the sensor-groups and the surface was pursued during the design phase. Consequently, a gap width between the sensor-boards and the cavity of only 1.5 mm was chosen. This minimal distance is required due to cavity comprehensive mechanical deviations of the cell. The measurement uncertainties caused by this minor offset compared to the desired sensor position directly at the cavity surface is approximated by a simulation model. For this purpose, the magnetostatic solver Pandira of the LAACG Poisson Superfish collection of programs for an applied stray field by a Helmholtz coil with a radius of 150 mm is used. For the equator (Group 5) a deviation of measurement results between the actual sensor-group position and the nearest cavity surface of about 6 % is predicted by the model.
To identify and solve possible technical issues of the system before the series production of the sensor-boards starts, two prototypes of the sensor-board printed circuit boards (PCB) were manufactured. During the PCB assembly of the first sensor-board (sensor-board I) a ferromagnetic material was identified in the selected Ceramic and Tantalum capacitors. Therefore, only one backup capacitor pair at the upper-right board-corner was populated during the assembly of the second PCB (sensor-board II) to prevent a parasitic drag of the later measurements.

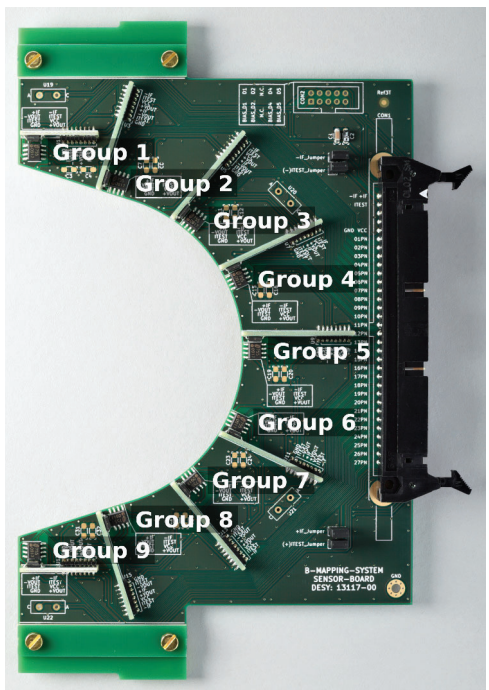

Figure 1: Second prototype of the DESY sensor-board design. The backup capacitors of each individual sensor are not populated due to a contained ferromagnetic material.

* This work was supported by the Helmholtz Association within the topic Accelerator Research and Development (ARD) of the Matter and Technologies (MT) Program.
† Jonas.Wolff@desy.de

ISBN: 978-3-95450-233-2 ISSN: 2673-5504 doi:10.18429/JACoW-SRF2021-SUPTEV009

Signal Processing

Mainly to extensively reduce the number of required cable feedthroughs, the differential sensor signals are already digitized inside of the cryostat. For this purpose evaluation-boards equipped with nine signal conditioning 24 bit analog-to-digital converters (ADC) of type Analog Devices AD7714 [8] were developed and are shown in Fig. 2. Each ADC provides three fully differential inputs used to digitize the signals of a single sensor-group. Additionally, an included programmable gain amplifier and a digital filter are used to cover the full sensor signal resolution. This is especially important when the system is used to measure flux changes of the residual background flux of less than 200 nT [5] during the T_c-transition. All ADCs on one sensor-board are controlled by a single ATMEL ATmega32 microcontroller. On request by an external computer, this microcontroller forwards the digitized sensor signals over a RS485 bus. Since a too high unit load [9] at the RS485 bus must be avoided, the network is split into two independent strings of 24 evaluation-boards each. The two half-duplex RS485 networks are organized in a master-slave framework between the external computer and the evaluation-boards as a measure to prevent data corruption.

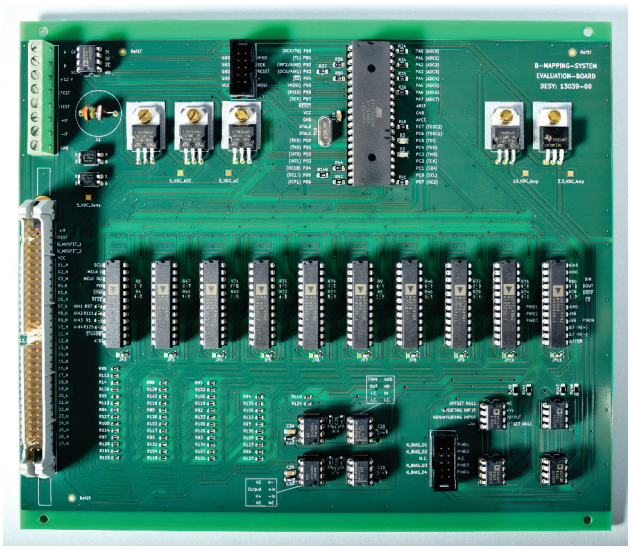

Figure 2: Custom-built 27-channel evaluation-board to digitize the differential output signals of a single sensor-board inside of the cryostat (mounted under the cryostat lid). The very right ADC is used to digitize the photodiode signals pre-conditioned by KEK design based transimpedance amplifiers.

To optimize the SNR, the PCB ground plane was separated into a digital and an analog region, the supply voltages were independently stabilized by fixed voltage regulators and measures for crosstalk prevention were taken. Following the recommendation in [10] for voltage references for 16+ bit ADCs, the output voltage is post-filtered by a low-pass filter followed by an impedance converter to further reduce the output noise.

Radiation Detection

To enable spatial measurements of field emission or multipacting related radiation in vicinity of the cavity cell, four of the later 48 sensor-boards will be equipped with Hamamatsu S6775 photodiodes [11]. By this approach, an undesired shielding by the surrounding buildup and hence a consequent reduction of the sensitivity and the threshold can be avoided.

Supplementary, the photodiodes will be used to allocate possible radiation related malfunctions of the AMR-sensors to their source. Radiation measurements with the selected type of photodiodes as well as with several alternatives were already successfully performed at INFN, JLAB, KEK and DESY [12–15]. The required signal processing circuitry is based on a KEK design of a transimpedance amplifier and located on the evaluation-boards (only populated if needed).

SENSOR CALIBRATION

The AMR-sensors at each sensor-board are individually calibrated by a housing-included test coil to induce a defined magnetic field. This field can be adjusted by the coil current I_{Test} within a range of ±200 mA at a typical magnetic field strength of 0.35 A/m/mA. According to the data sheet [2] the test field may show a component spread of 0.25 to 0.45 A/m/mA. The wide range and the consequently unknown individual value makes the test coil unsuitable for the sensor calibration. Indeed, during a test series at HZB [4] a way lower spread of (0.249 ± 0.12) µT/mA was determined. During the first performance tests at DESY this latter value is used for the sensor calibration.

Before every test-run, a calibration curve is recorded for each sensor by a stepwise increase of the test coil current within a range of 0 to 200 mA and a stepwidth of 5 mA to minimize the noise impact with the help of a consequent linear fit. Exemplary, one of these curves is shown in Fig. 3. Slope and voltage offset are determined by the linear fit.

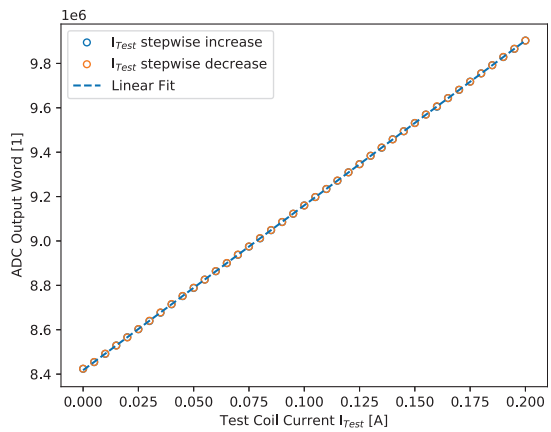

Figure 3: Linear fit to a stepwise increased test coil current I_{Test} within a range of 0 to 200 mA used for the sensor calibration. To detect during the current rise possibly magnetized components in vicinity of the specific sensors an identical stepwise decrease is performed afterwards.

ISBN: 978-3-95450-233-2 ISSN: 2673-5504 doi:10.18429/JACoW-SRF2021-SUPTEV009

FIRST PERFORMANCE TEST

For the first performance test in the vertical test stand sensor-board II was mounted on the large grain cavity 1DE21. This setup is surrounded by a Helmholtz coil with a coil radius of 150 mm to apply a magnetic stray flux of optionally 1 µT or 10 µT during the measurements. Since the Helmholtz coil radius is too small to be centred around the cavity for the given setup, it was mounted with an offset of 29 mm from the cavity axis as shown in Fig. 4. The temperature of the cavity surface is monitored by three Lake Shore Cryotronics Cernox CX1030 sensors attached to the cavity at the equator (Temp 2) as well as with a distance along the cavity axis to the equator of ± 139 mm.

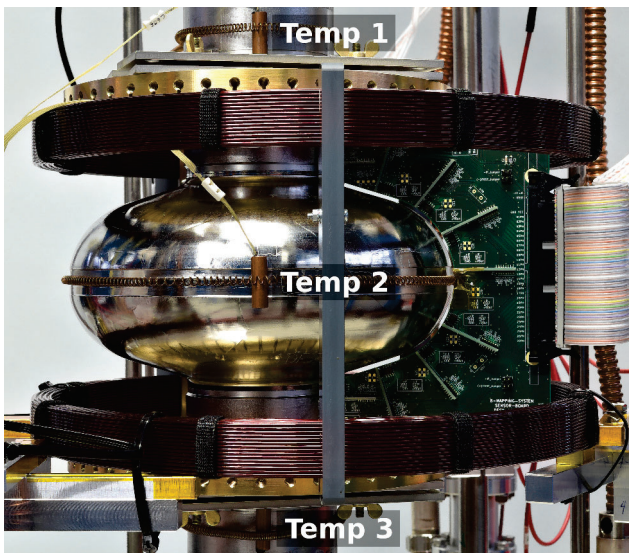

Figure 4: Measurement setup: 1.3 GHz TESLA-Type single-cell SRF cavity (1DE21 - large grain material) equipped with only one sensor-board and a Helmholtz coil to apply a magnetic stray field. The cavity temperature is monitored by three Lake Shore Cryotronics Cernox CX1030 temperature sensors (Temp 1-3).

Because of an unknown output voltage offset of the AMR-sensors, a static background flux can only be determined by a sample pair with two oppositional flip coil current pulses of same length and magnitude. Unfortunately, during former tests at HZB [6] with various coil currents and pulse lengths an increasing dispersion was observed for cryogenic temperatures. Hence, by this setup the residual background flux can not be determined inside of the cryostat. Nevertheless, this type of measurements was repeated with the DESY setup to reproduce the HZB results. Due to the power supply's output capacity, the flip coil current is not bounded by a selected current limitation for pulse lengths in the lower microsecond regime. Consequently, a series resistor was added to the supply wire of the flip coil series to prevent a current rise above the sensor specification [2], since the material purity related resistivity drop was unknown before the first cooldown. The added series resistor lead to a flip coil current of 0.41 A at room temperature. Before the cooldown, the system was first calibrated with a sampling rate of 50 Hz in bipolar mode and using a gain of 16. Subsequently, the cooldown was started with a gradient of approximately −60 K/h and samples shown in Fig. 5 with a toggling flip coil current I_F were taken. After each current direction change, five pulses were awaited before a sample was logged. The cooldown was paused at 12 K to ensure that the temperature of the complete cavity is above T_c before the start of the following measurement. Similar to the measurements at HZB, a random drift was observed during the cooldown as shown in Fig. 5 and a high standard deviation σ of up to 6.5 µT ($\overline{B}$: 8.7 µT) was evaluated. Thus, the observations at HZB could be reproduced. Subsequent to the cooldown, the residual resistance of the series connection of all 27 flip coils and the connection cable was measured for sensor-board I (13.9 Ω) [1] mounted only for this purpose about 0.5 m above the setup. Then, the protection resistor of the flip coil series of sensor-board II was removed and the related voltage was adjusted to drive 1 A current pulses with a pulse length of 10 µs (t_{down} > 400 µs). A series of flip coil pulses was awaited before the flip coil current was switched off. Afterwards the first cooldown from 12 K to 6 K was started with a gradient of −3 K/h and a magnetic stray flux of 10 µT applied by the Helmholtz coil. The measured flux distribution during the T_c-transition as well as in the initial and the final state are spatially visualized in Fig. 6. By a comparison of the related sensor-groups at the upper and lower half cell grain boundary dependent differences of the absolute value and the vector orientation can be observed. When the trends of the Cartesian vector components of a single sensor-group are individually examined as plotted in Fig. 7 for Group 5 together with the measured temperatures (Temp 1-3), an increased noise level of the Z-AMR-sensor is conspicuous. This increased noise level was caused by the Helmholtz coil

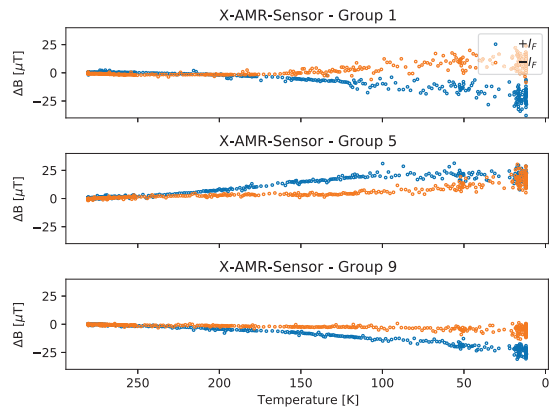

Figure 5: Measured relative magnetic flux ΔB as a function of the temperature during the cooldown. The temperature dependent flip coil current I_F of 0.41 to 0.73 A was toggled with a pulse length of 10 µs. After each current direction change, five pulses were awaited before a sample was logged.

[1] This measurement was later repeated at a board temperature of 1.8 K and a residual series resistance of 4.0 Ω was measured. Due to the position offset the exact board temperature of the former measurement is unknown.

ISBN: 978-3-95450-233-2 ISSN: 2673-5504 doi:10.18429/JACoW-SRF2021-SUPTEV009

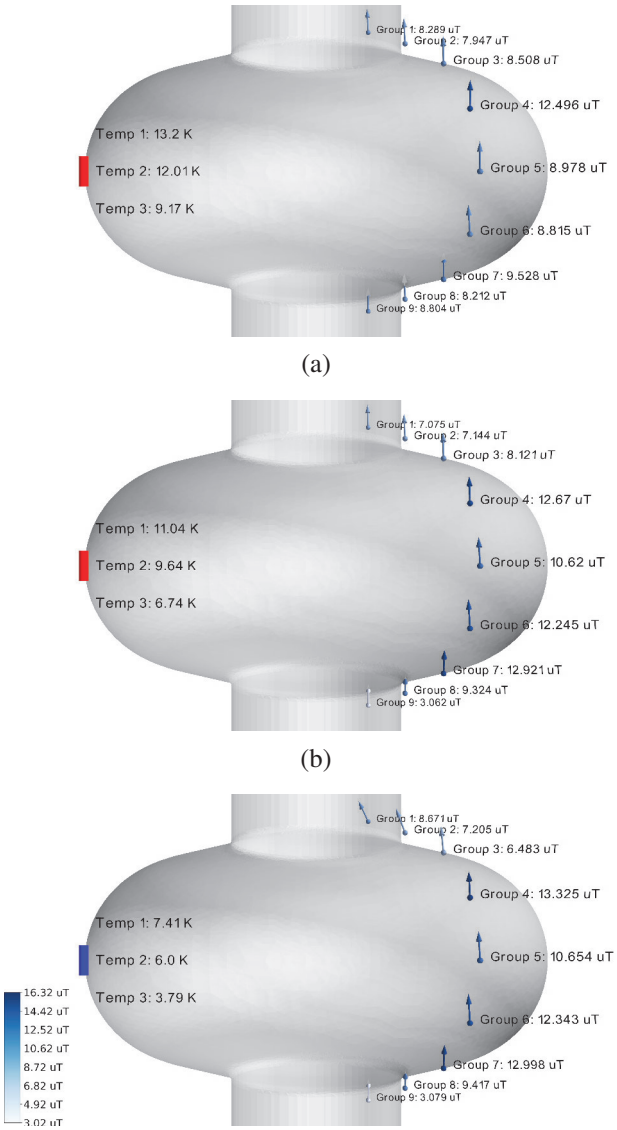

Figure 6: T_c-transition B-map of cavity 1DE21 (large grain material) with an applied magnetic flux of 10 µT: (a) Initial state before the T_c-transition at 12 K (Temp 2); (b) Equator at T_c (9.2 K) process of flux expulsion / trapping can be observed at the lower half cell (see orientation and absolute value of Group 5-9); (c) Complete cavity below T_c. Niobium grain boundary dependent differences in flux trapping / expulsion behavior can be observed by comparing the groups at the upper and the lower half cell.

current (verified by a consequent similar test-run with no applied stray flux). For this reason, the power supply will be replaced by a better stabilized current source for the future measurements.

Due to the delay of approximately ten minutes between the detection of the T_c-transition by the AMR-sensors and the corresponding temperature (Temp 2) an inclined transition of the cavity can be assumed. After this test-run with an applied

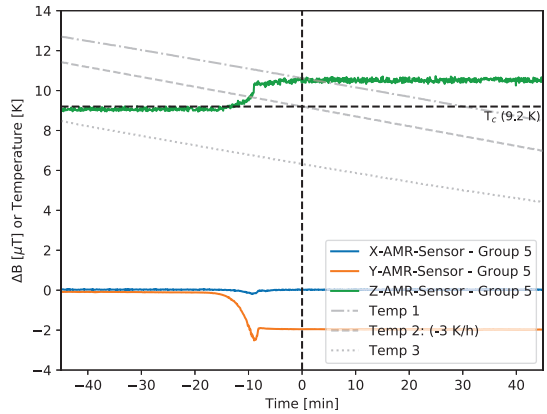

Figure 7: Relative magnetic flux change of Group 5 (located at the equator) during the T_c-transition plotted separately for the Cartesian vector components. The increased noise of the Z-AMR-Sensor is caused by the Helmholtz coil current.

stray flux of 10 µT, the cavity was warmed up to 12 K and the procedure was repeated twice with a stray flux of 1 µT and with no stray flux (Helmholtz coil current switched off). As a measure for the signal noise, the standard deviations σ and the corresponding mean values $\overline{B}$ were computed for the sensor-groups and the individual channels. For the last test-run from 12 K down to 6 K without an applied stray flux a low but highly channel dependent standard deviation σ within in a range from 3 nT ($\overline{B}$: 48 nT) to 19 nT ($\overline{B}$: 447 nT) was evaluated. As shown in Fig. 8, the system can even detect T_c-related magnetic flux changes near the cavity surface of the residual background field. An overview of the sensor-group related standard deviations σ for all test-runs is given in Table 1. The low noise contribution by the Helmholtz coil current of the sensor-groups in vicinity of the drift tube is caused by a partial flux expulsion related shielding effect of the cavity cell. This assumption was verified by a comparison with the respective standard deviations σ before the T_c-transition listed in Table 2.

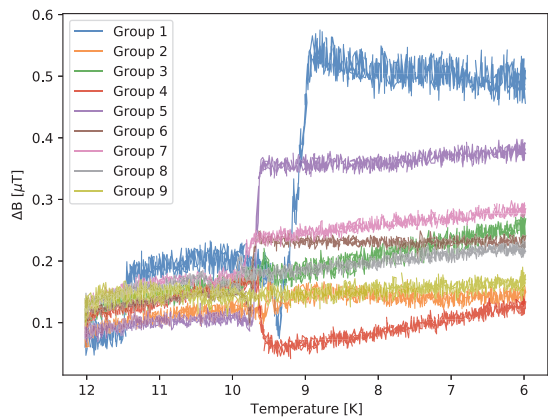

Figure 8: Absolute values of the sensor-groups as a function of the equator temperature (Temp 2) for the last test-run with no applied magnetic stray flux by the Helmholtz coil.

ISBN: 978-3-95450-233-2 ISSN: 2673-5504 doi:10.18429/JACoW-SRF2021-SUPTEV009

Table 1: Overview of the standard deviations σ and the corresponding mean values $\overline{B}$ of the sensor-groups (Gr) computed by the last 200 samples (below T_c) of each test-run.
(The results are sorted by the particular applied magnetic stray flux by the Helmholtz coil (HC)).

Gr	0 µT by HC		1 µT by HC		10 µT by HC	
	$\overline{B}[nT]$	$\sigma[nT]$	$\overline{B}[\mu T]$	$\sigma[nT]$	$\overline{B}[\mu T]$	$\sigma[nT]$
1	493.7	17.9	0.5	17.7	8.7	14.1
2	142.2	8.4	0.4	36.6	7.2	8.1
3	252.4	10.4	0.8	63.8	6.5	43.0
4	126.1	7.3	1.6	110.3	13.3	89.7
5	377.9	7.9	1.5	74.7	10.7	59.5
6	231.3	5.5	1.5	77.8	12.2	56.5
7	281.2	6.2	1.2	75.3	12.9	58.3
8	220.2	6.4	0.7	37.9	9.4	31.0
9	164.4	8.0	0.2	15.9	3.1	19.9

Table 2: Overview of the standard deviations σ and the corresponding mean values $\overline{B}$ of the flux shielding effected sensor-groups (Gr) computed by the first 200 samples (above T_c) of each test-run.
(The results are sorted by the particular applied magnetic stray flux by the Helmholtz coil (HC)).

Gr	0 µT by HC		1 µT by HC		10 µT by HC	
	$\overline{B}[nT]$	$\sigma[nT]$	$\overline{B}[\mu T]$	$\sigma[nT]$	$\overline{B}[\mu T]$	$\sigma[nT]$
1	96.2	36.7	0.8	54.1	8.3	52.5
2	91.2	11.3	0.8	40.3	8.0	42.2
8	140.9	9.7	0.9	28.1	8.2	31.8
9	139.0	12.4	0.9	35.6	8.8	39.1

CONCLUSION

A new approach of a B-mapping system to enable high-resolution spatial magnetic flux measurements along the outer surface of 1.3 GHz TESLA-Type single-cell SRF cavities has been developed at DESY. To extensively reduce the number of required cable feedthroughs the system digitizes the differential sensor signals already inside of the cryostat. Due to the consequently reduced thermal noise, shortened analog signal lines and the Mu-metal shielding of the test stand also the SNR can be improved by this approach. During a first performance test, the system was successfully tested at temperatures down to 1.8 K. For the different channels a low but highly channel dependent standard deviation σ within a range of 3 nT ($\overline{B}$: 48 nT) to 19 nT ($\overline{B}$: 447 nT) was evaluated.
The system can be used to investigate the flux trapping behavior even by only the residual magnetic background field. To improve the accuracy of the AMR-sensor calibration the series connection of the test coils will be separated into independent lines for each axis to reduce the stray impact from other test coils.

ACKNOWLEDGEMENTS

We would like to thank our colleagues - F. Kramer and O. Kugeler from Helmholtz-Zentrum Berlin, and R. Apel, C. Bate, T. Buettner, C. Ceylan, K. Demmler, A. Doerner, L. Ebeling, N. Engling, J. Eschke, I. Flick, S. Harder, A. Heck, G. Kacha Deyu, D. Klinke, D. Kostin, R. Monroy-Villa, M. Mommertz, A. Muhs, T. Nagel, J. Schaffran, R. Schappeit, L. Trelle, H. Weise, M. Wenskat, O.-C. Zeides and J. Ziegler from DESY - for their support of this project.

REFERENCES

[1] B. Schmitz, K. Alomari, J. Köszegi, O. Kugeler, Y. Tamashevich, and J. Knobloch, "Setup of a Spatially Resolving Vector Magnetometry System for the Investigation of Flux Trapping in Superconducting Cavities," May 2017.
[2] *AFF755B MagnetoResistive Field Sensor*, Sensitec, Jul. 2018.
[3] S. Posen *et al.*, "Efficient expulsion of magnetic flux in superconducting radiofrequency cavities for high Q0 applications," *Journal of Applied Physics*, vol. 119, no. 21, p. 213 903, 2016. doi:10.1063/1.49530.87
[4] B. Schmitz, J. Köszegi, K. Alomari, O. Kugeler, and J. Knobloch, "Magnetometric Mapping of Superconducting RF Cavities," *Review of Scientific Instruments*, vol. 89, Apr. 2018. doi: 10.1063/1.5030509
[5] S. Huang, T. Kubo, and R. Geng, "Dependence of trapped-flux-induced surface resistance of a large-grain Nb superconducting radio-frequency cavity on spatial temperature gradient during cooldown through Tc," *Physical Review Special Topics - Accelerators and Beams*, vol. 19, Aug. 2016. doi:10.1103/PhysRevAccelBeams.19.082001
[6] F. Kramer, "Mapping Trapped Flux and the related Surface Resistance in Superconducting Cavities," Master's thesis, University of Siegen, Jul. 2019.
[7] D. Longuevergne and A. Miyazaki, "How can geometry impact the magnetic flux trapping of superconducting accelerating cavities," Sep. 2020.
[8] *AD7714*, 3V/5V, CMOS, 500 µA Signal Conditioning ADC, 1998.
[9] "Electrical Characteristics of Generators and Receivers for Use in Balanced Digital Multipoint Systems," TIA, Tech. Rep., Mar. 1998, TIA/EIA-485-A.
[10] *Tips and Tricks for Designing with Voltage References*, Texas Instruments, 2021.
[11] *Si PIN photodiodes S2506/S6775/S6967 series*, Hamamatsu, May 2021.
[12] M. Bertucci *et al.*, "Quench and field emission diagnostics for the ess medium-beta prototypes vertical tests at lasa," May 2017.
[13] A. Palczewski and R. Geng, "Evaluation Of Silicon Diodes As IN-SITU Cryogenic Field Emission Detectors For SRF Cavity Development," *IPAC 2012 - International Particle Accelerator Conference 2012*, Jan. 2012.
[14] H. Sakai *et al.*, "Field emission studies in vertical test and during cryomodule operation using precise x-ray mapping system," *Physical Review Accelerators and Beams*, vol. 22, Feb. 2019. doi: 10.1103/PhysRevAccelBeams.22.022002
[15] T. Nagel and M. Wenskat, *Private communication*, 2020.